

The University of Akron

IdeaExchange@UAkron

Williams Honors College, Honors Research
Projects

The Dr. Gary B. and Pamela S. Williams Honors
College

Spring 2022

Comparing Galvanic Corrosion Rates Predicted from Polarization Curves with Empirical Data from a Carbon Steel and Monel Couple for a Various Geometries

Michael Hinnebusch
mah267@uakron.edu

Follow this and additional works at: https://ideaexchange.uakron.edu/honors_research_projects



Part of the [Other Chemical Engineering Commons](#), and the [Other Engineering Commons](#)

Please take a moment to share how this work helps you [through this survey](#). Your feedback will be important as we plan further development of our repository.

Recommended Citation

Hinnebusch, Michael, "Comparing Galvanic Corrosion Rates Predicted from Polarization Curves with Empirical Data from a Carbon Steel and Monel Couple for a Various Geometries" (2022). *Williams Honors College, Honors Research Projects*. 1581.

https://ideaexchange.uakron.edu/honors_research_projects/1581

This Dissertation/Thesis is brought to you for free and open access by The Dr. Gary B. and Pamela S. Williams Honors College at IdeaExchange@UAkron, the institutional repository of The University of Akron in Akron, Ohio, USA. It has been accepted for inclusion in Williams Honors College, Honors Research Projects by an authorized administrator of IdeaExchange@UAkron. For more information, please contact mjon@uakron.edu, uapress@uakron.edu.

**Comparing Galvanic Corrosion Rates Predicted
from Polarization Curves with Empirical Data from
a Carbon Steel and Monel Couple for Various
Geometries**

Micheal Hinnebusch

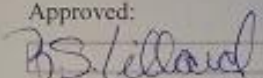
Department of Chemical, Biomolecular and Corrosion
Engineering

Honors Research Project

Submitted to

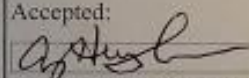
*The Williams Honors College
The University of Akron*

Approved:

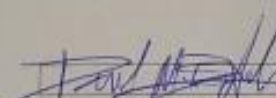
 Date: 5/4/22
Honors Project Sponsor (signed)

R.S. Lillard
Honors Project Sponsor (printed)

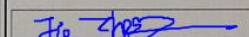
Accepted:

 Date: 5/5/22
Honors Department Advisor (signed)

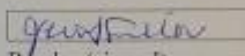
Hengbo Cong
Honors Department Advisor (printed)

 Date: 5/5/22
Reader (signed)

D. Bastidas
Reader (printed)

 Date: 05/05/2022
Department Chair (signed)

J. Zheng
Department Chair (printed)

 Date: 5/4/22
Reader (signed)

J. Lillard
Reader (printed)

Contents

Abstract	3
Introduction	3
Experimental	4
Results	7
Discussion	28
Conclusion	28
Works Cited	29

Abstract

The objective of this investigation was to compare the galvanic corrosion rate of carbon steel C1018 and Monel K-500 alloy in a bolt and plate geometry to that derived using Tafel plots. This was achieved using carbon steels sheets of steel with a pair of with varying the number of Monel bolts and varying spacing. It was found that the carbon steel plates do not corrode uniformly. This can create issues when using Polarization curves to assume galvanic corrosion rate of a carbon steel and Monel system. The geometry of the bolts can further affect this corrosion rate and make the system more complicated.

Introduction

Galvanic corrosion occurs when two dissimilar metals are coupled together and exposed to a corrosive environment [1,2]. When galvanic corrosion occurs, the more noble metal induces its current onto the less noble metal causing corrosion. This will increase the corrosion rate of the less noble metal. Being able to quantify this corrosion rate is commonly done through polarization curves (Tafel plots). Taking the polarization curves of each individual metal and finding where the two metals intersect allows someone to empirically estimate the corrosion rates of the coupled system.

Polarization curves are a common way of measuring the corrosion rates of a metal in an aqueous solution. Polarization curves work by applying a potential the metal (working electrode) and measuring the resulting current through an auxiliary electrode in an aqueous solution. There are a few drawbacks with measuring corrosion rate using this method. The first is that faster potential scan rates will generally yield higher measurements of current, and the shapes of the curves may have different rates [1]. The second is that measured currents may vary depending on the starting potential of the scan. The third is that corrosion film build up for galvanically coupled systems in long term exposure will be different than the ones measured using polarization behaviors. The final drawback is that the ohmic resistance of the electrolyte will influence coupled polarization behavior and scan rate in a potentiodynamic test. Despite these drawbacks, polarization curves give a reliable enough measurement to predict corrosion rates of galvanically connected systems [2,3].

Monel is a copper-nickel alloy used in marine applications [4]. The nickel present in Monel makes it more noble and corrosion resistant by forming stable oxides that gives it a slower corrosion rate compared to steel. Monel is used in marine environments to protect structures in shipbuilding, offshore, power, and desalination industries. It is commonly used in military submarine service due to its higher strength and maximum allowable flow rate.

To calculate the anticipated mass loss of the coupons, Faradays Law was used to convert the corrosion current density (i_{corr}) of carbon steel and Monel coupled together. [5] Faraday's constant was used along with unit conversions of molecular weight, area of exposure, time of exposure, and number equivalent of electrons transferred per mole to determine the expected mass loss. **Equation 1** shows the use of Faraday's Law and unit conversion to determine the anticipated mass loss.

Mass Loss from corrosion current density using Faraday's Law

$$\text{mass loss (g)} = \frac{i_{\text{corr}}(\frac{A}{\text{cm}^2}) * \text{time}(s) * \text{Molecular Weight}(\frac{g}{\text{mol}}) * \text{Area}(\text{cm}^2)}{\text{Number Equivalent}(\frac{\text{equiv}}{\text{mol}}) * \text{Faraday's constant}(\frac{C}{\text{equiv}})} \quad (1)$$

Below are the known compositions of carbon steel C1018 and Monel K-500 taken from academic sources.

Table 1: The table below shows the composition of Carbon Steel C1018 [6].

Element	C	Mn	P	S	Mo	Si	Fe
wt%	0.18	0.90	0.017	0.012	0.018	0.044	Bal.

Table 2: The table below shows the composition of Monel K-500 [7].

Element	Ni	Mn	Fe	Si	Al	Ti	Cu
Wt%	61.8	1.25	2.0	1.0	3.5	0.95	Bal

Experimental

To create the Monel and carbon steel galvanic couple, carbon steel C1018 sheet metal was used. The carbon steel sheet had a width of 2.5 cm. Twelve specimens were then cut to a length of 6.85 cm. Each bolt geometry had three samples. For the single bolt coupons, a 6.2 mm (1/4") bolt hole was drilled in the center of the coupon. For the "Negative 5mm" geometry two 6.2mm (1/4") holes were drilled with a center-to-center distance of 16.9mm. For the "Positive 5mm" geometry two 6.2mm (1/4") holes were drilled with a center-to-center distance of 26.9mm. For the "Positive 15mm" geometry two 6.2mm (1/4") holes were drilled with a center-to-center distance of 36.9mm as shown in Figure 1

To prepare the surfaces of the carbon steel coupons for testing, the bare metal of the carbon steel needed to be exposed and polished. This was done using a Struers Tegramin-30 polishing machine, starting at 240 SiC paper and finishing at 600 SiC paper while using water as a lubricant. After each polishing cycle, deionized (DI) water and ethanol were used to rinse off the surfaces before using compressed air to dry the surfaces. To prepare the surfaces of the Monell bolts, a Dremel with a steel wire brush was used to remove any oxide film and expose the pure alloy metal underneath. Once polished and dried the test coupons had their mass measured for weight loss analysis.

To isolate the geometry of the affected region, a circular brass punch tools were used to cut 22.0mm diameter circles of green 3M Electroplaters tape. The diameter of the circles creates an equivalent to the area of exposure to the carbon steel surface as there is to the area of the Monel bolt heads. The green circular tape was layered over the center of the bolt holes and smoothed out to remove air bubbles with the rounded back end of a razor blade. Red Glyptal 1201 Red Enamel (a xylene-based paint) was then applied to the top and sides of the carbon steel coupons and allowed to cure for 24 hours. The next day the green tape was then removed from the top of the coupons and the Monel bolts and nuts were tightened by hand using wrenches on the carbon steel coupons through the bolt holes. The backside of the coupon and Monel bolt nuts and threads were then painted with the same paint. The coupons were then allowed 48 hours to fully cure with inspections to ensure that all areas that should be coated were coated.

A modified experiment was conducted on one “Negative 5mm” and “One-hole” test specimen. For the “Negative 5mm” coupon, the entire top surface of the coupon was left uncoated to and a ratio of exposed carbon steel area to Monel bolt head area was calculated. An equivalent ratio was then used to calculate the area of exposure for the “One-hole” bolt coupon with having a length of 3.16mm of exposure to the 2.6mm of width of the plate with the center of the area being the with the center of the bolt.

A simulated saltwater solution was prepared to act as the aggressive environment to galvanically corrode the carbon steel coupons. One liter of ASTM standard D1141-52 test solution was prepared to test two coupons for the 8-day exposure. The solution had its pH adjusted to 8.4 using 0.1M HCl and 0.1M NaOH and a calibrated Orion Star A211 pH probe. The solution was poured into 3-liter wide well glass dish and flexible PVC tubing connected to a fish pump was added to constantly aerate the solution by running with gentle stream of a couple bubbles per second. The coated galvanic coupons were added to the solution and the time and date recorded to ensure the coupons were removed after completing the 8-day exposure. A red sharpie was used to mark the initial water line of the system and DI water was used to replace any evaporated water during exposure.

Once the exposure was completed, the test specimens were removed from the solution and the surface rust of the carbon steel was removed with DI water and gentle brushing of a toothbrush. Ethanol was used as the final rinse before are drying the surfaces. The coupons were then submerged into a xylene bath for a few hours to easily remove the coating from the coupons. The Monel bolts were then carefully removed using a wrenches and final weight measurements were taken of the coupons.

As Alicona Infinite Focus G5 3D microscope was used to measure the surface roughness of the coupons and to assess the corrosion damage. A “cross” like pattern was done to measure the depth of corrosion damage and geometry from the edge of the bolt hole towards the edge of the radius of the exposed circular region protected by the xylene paint. Surface roughness 3D scans were taken at the “12-”, “3-”, “6-”, and “9-o’clock” sections around the bolt hole for each bolt hole. These directions of scans allowed for making surface geometry measurements of the corrosion damage area in between the bolts, opposite of the bolts, and of the sides of the bolts. The scan width was 500 points. The surface was normalized using the rectangular planar tool in the software. Surface roughness profile was then used to calculate the volume of the mass loss of the coupons. **Equation 2** shows the equation used where “R” is outer radius, “r” is the inner radius, and “h” is the surface roughness that corresponds to the outer radius.

Volume Loss from linear profile Volume of a cylinder and Trapezoidal Rule

$$Volume (mm^3) = \Sigma\pi(R^2 - r^2) * h \quad (2)$$

The Polarization curves of **Figure 2** were provided to by Dr. R.S. Lillard. They were constructed over a four-day exposure at an Open Circuit Potential. Both the carbon steel and Monel samples were exposed to ASTM D1141-52 simulated saltwater water solution [8].

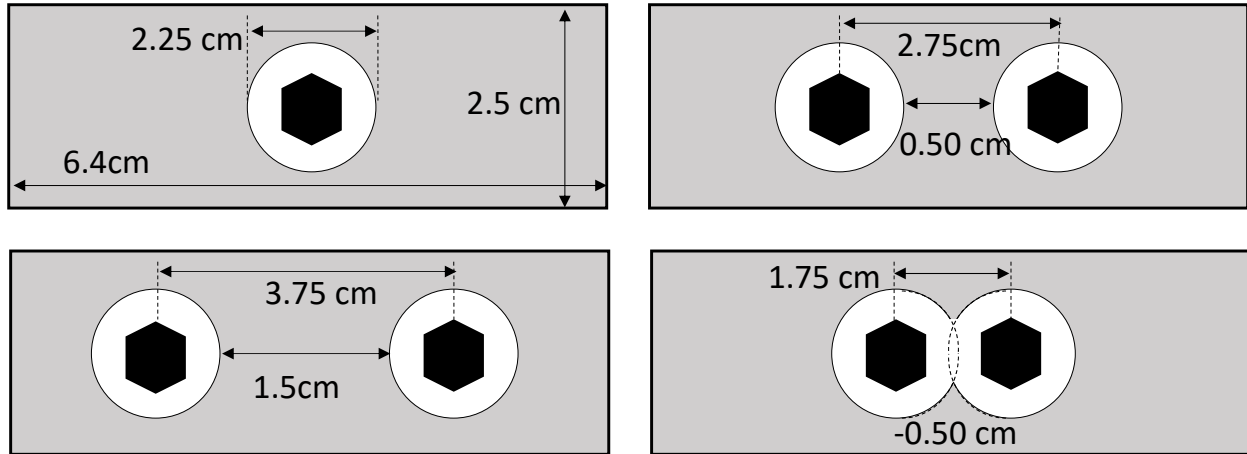


Figure 1: Diagram of the Monel bolt and carbon steel plate geometries used. The exposed steel area is represented by white circles around the hexagonal bolt. Bolt to steel area ratios were 1:1 except for the -0.50 cm configuration. The top left diagram is for the Single Hole Coupon. The top right diagram is for the Positive 5mm coupon. The bottom left diagram is for the Positive 15mm coupon. The bottom right diagram is for the Negative 5mm coupon.

Results

Below is the Polarization curves of carbon steel C1018 and Monel K-500 provided by Dr. Lillard. Both specimens were exposed to ASTM D1141-52 simulated ocean water. The curves were run during a four exposure at their open circuit potentials.

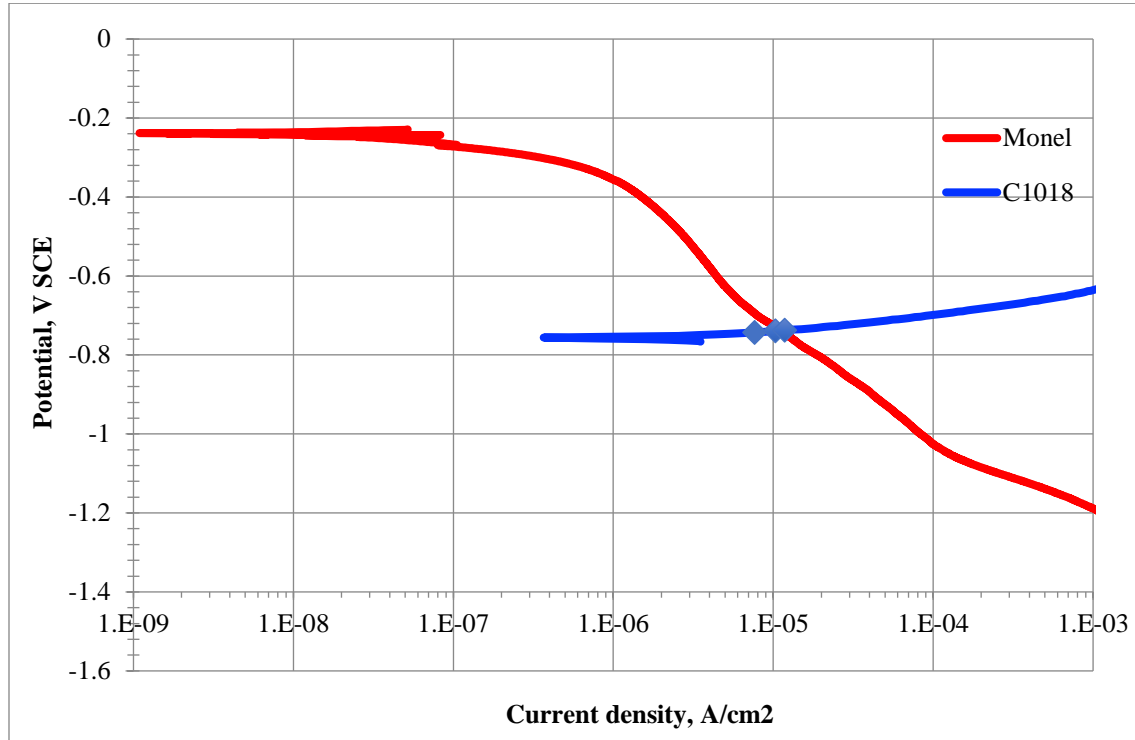


Figure 2: The figure above illustrates the 4-day open circuit potentiodynamic data collected of carbon steel 1018 and Monel exposed ASTM D1141-52 saltwater exposure.

Table 3: The table illustrates corrosion current density and corrosion potentials from the individual Tafel slopes data of carbon steel and Monel used for calculating the anticipated mass loss of the carbon steel and Monel coupons.

E_{couple} (V vs SCE)	-0.7388
i_{couple} (A/cm ²)	$1.109 \cdot 10^{-5}$

Table 4: This table illustrates the expected mass loss based on the area of exposure of the carbon steel and the corrosion current density of carbon steel and Monel galvanically coupled ($1.11 \cdot 10^{-5}$ A/cm²) derived from Tafel slopes data and using Faraday's Law.

i_{corr} : $1.11 \cdot 10^{-5}$ (A/cm ²)	Area (cm ²)	8-day Exposure Mass Loss (mg)
Single Bolt	2.49	3.68
Double Bolt (w/ overlap)	4.18	6.18
Double Bolt	4.98	7.36

Table 5: The table above shows the derived volume loss and mass loss from the 3D microscope surface roughness data.

	Volume Loss (mm ³)	Mass Loss (mg)
One Hole	1.686	13.24
Negative 5mm	2.552	20.03
Positive 5mm	3.042	23.88
Positive 15mm	2.424	19.03

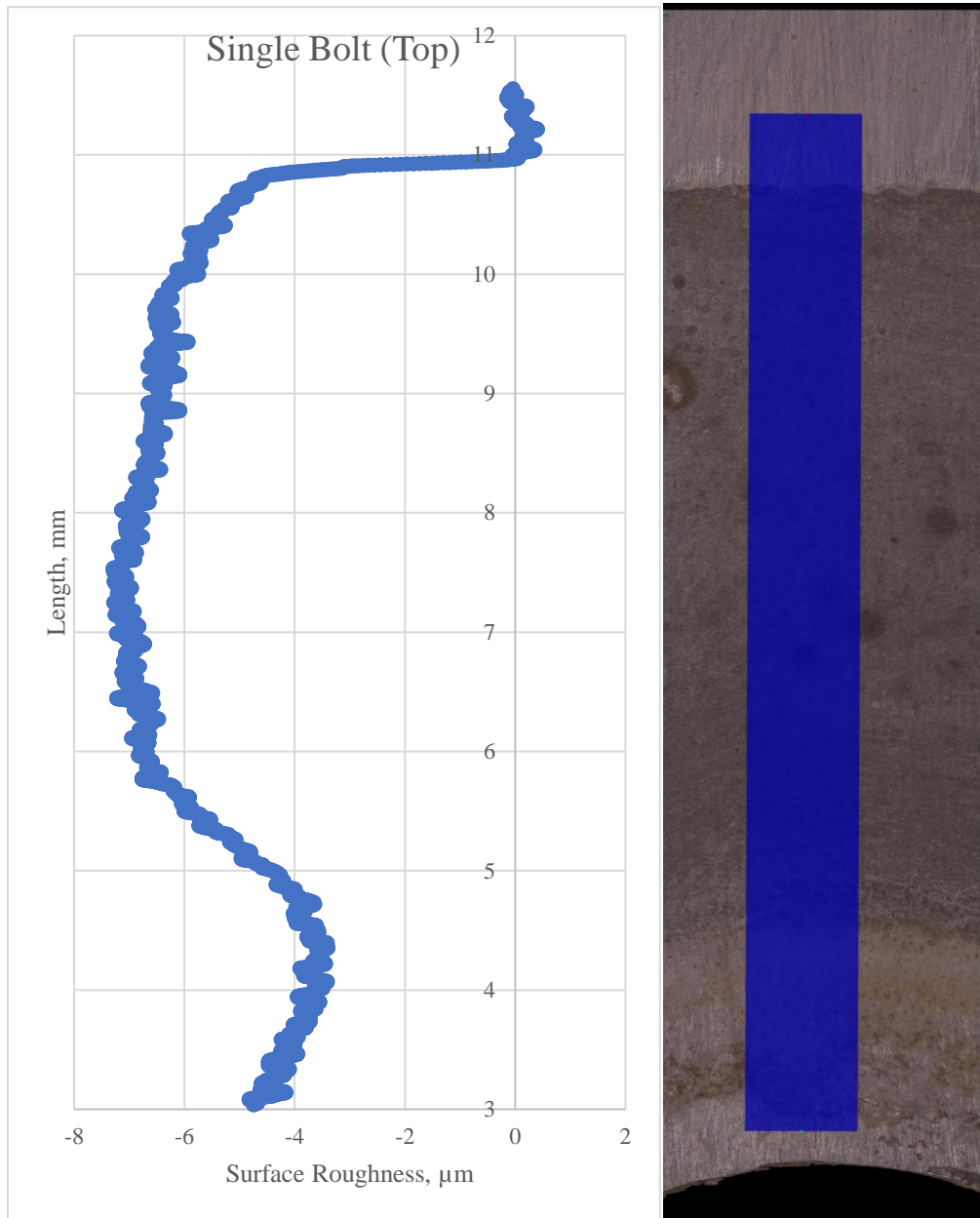


Figure 3: The above figures illustrate corrosion damage of the carbon steel of the top portion of the single bolt coupon using surface roughness measurements from the 3D microscope.

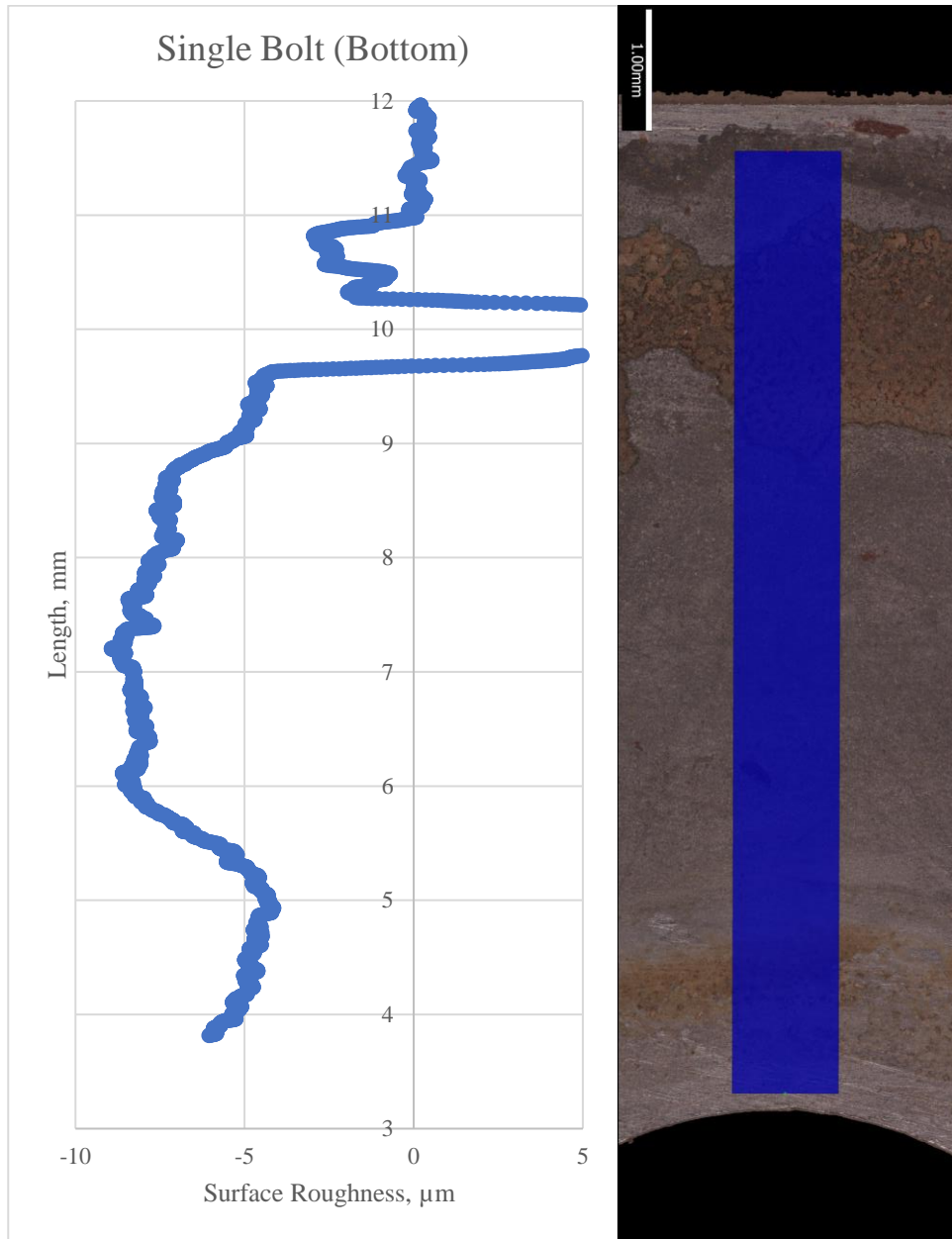


Figure 4: The above figures illustrate corrosion damage of the carbon steel of the bottom portion of the single bolt coupon using surface roughness measurements from the 3D microscope.

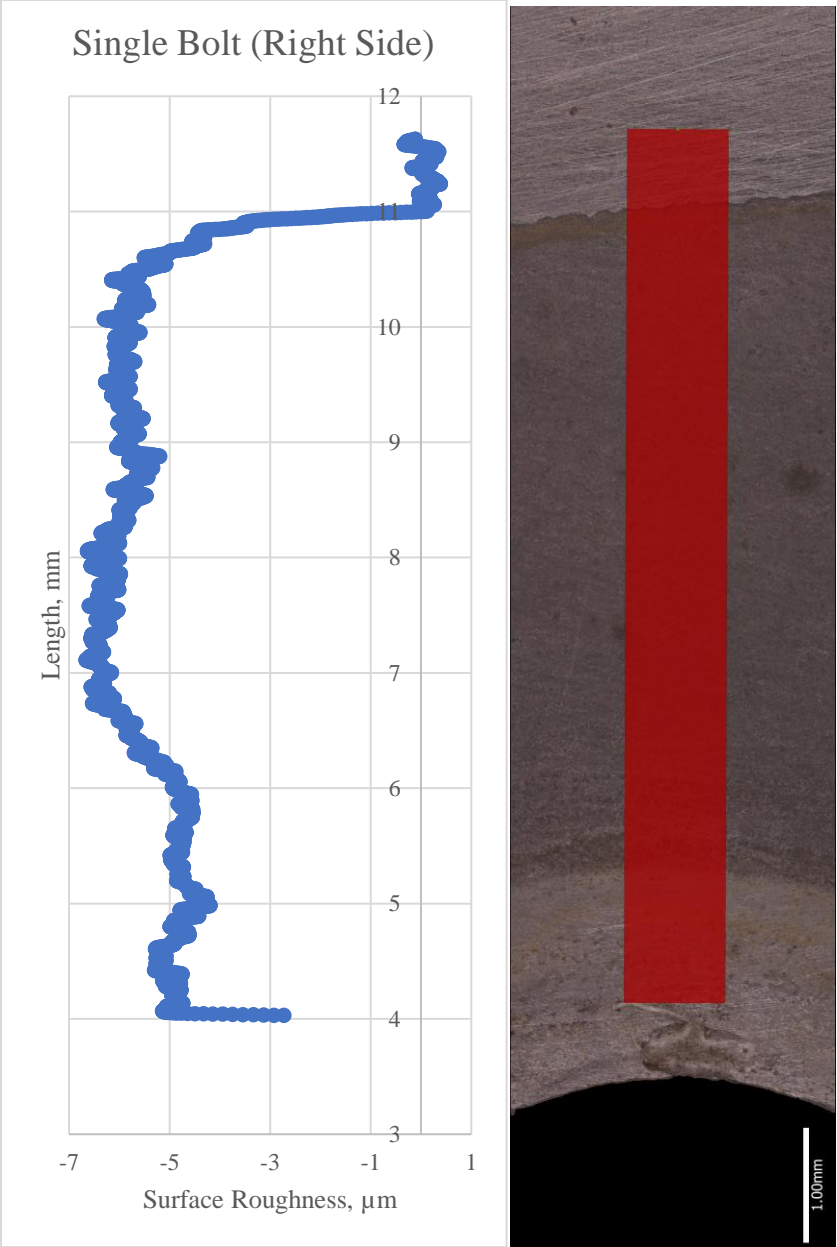


Figure 5: The above figures illustrate corrosion damage of the carbon steel of the right-side portion of the single bolt coupon using surface roughness measurements.

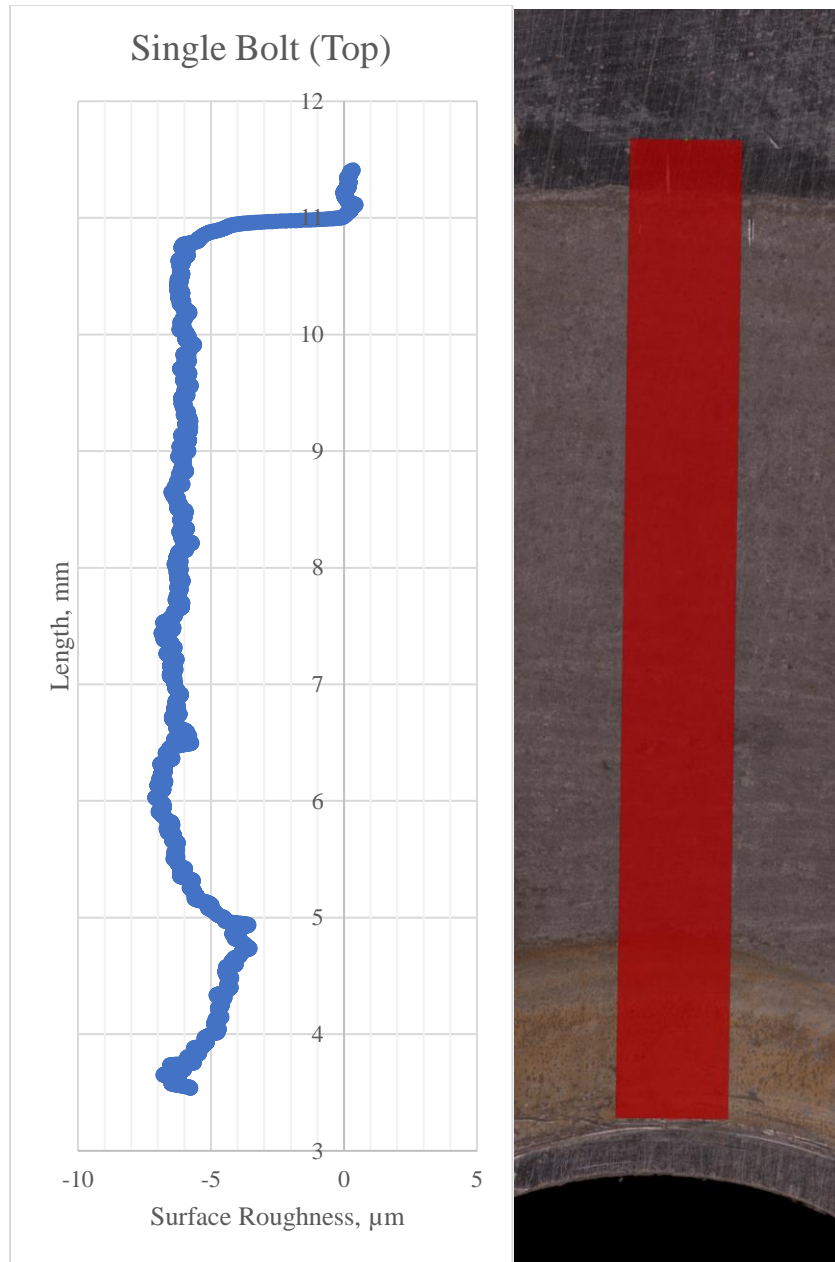


Figure 6: The above figures illustrate corrosion damage of the carbon steel of the top portion of the negative 5mm coupon using surface roughness measurements from the 3D microscope.

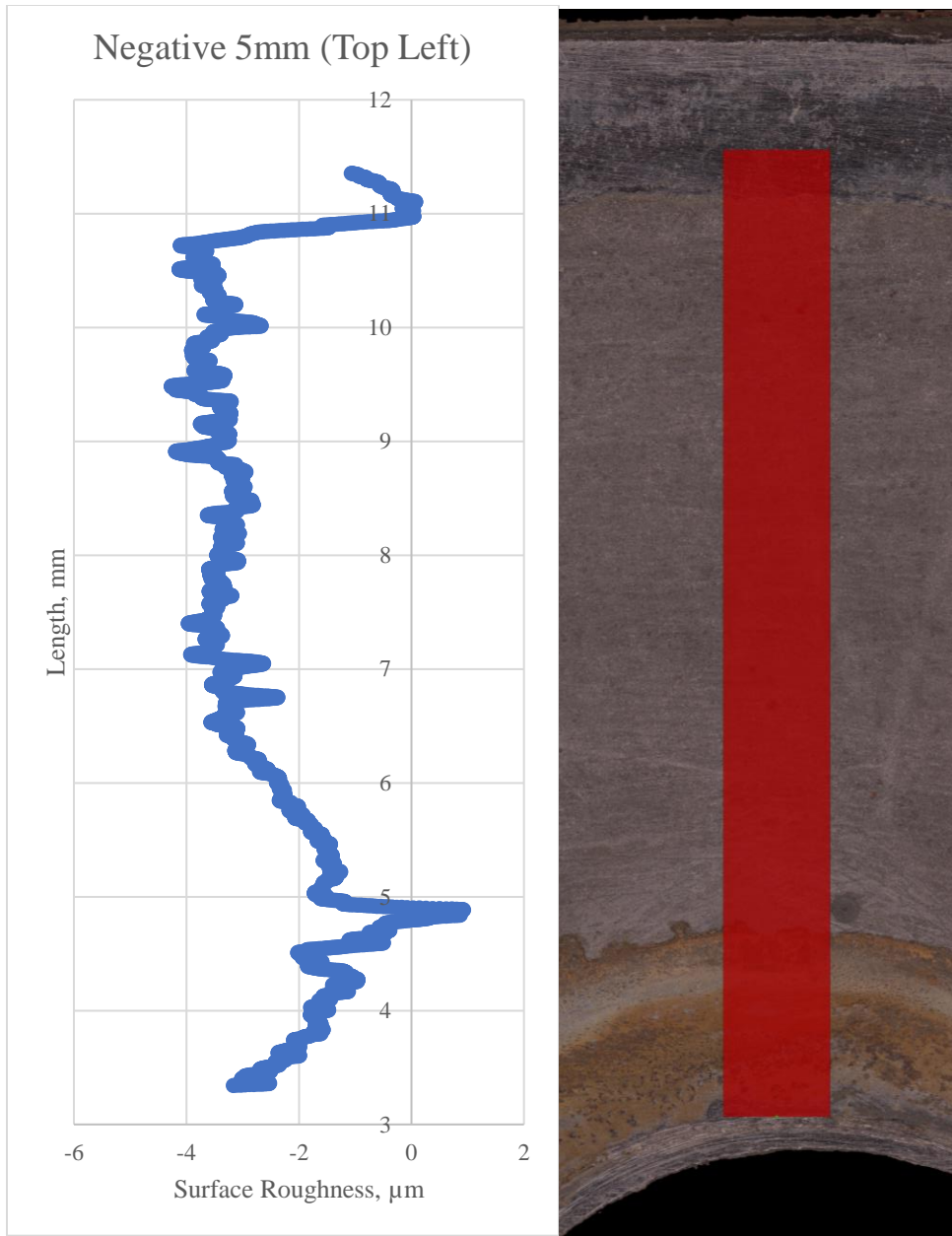


Figure 7: The above figures illustrate corrosion damage of the carbon steel of the top left portion of the Negative 5mm coupon using surface roughness measurements from the 3D microscope.

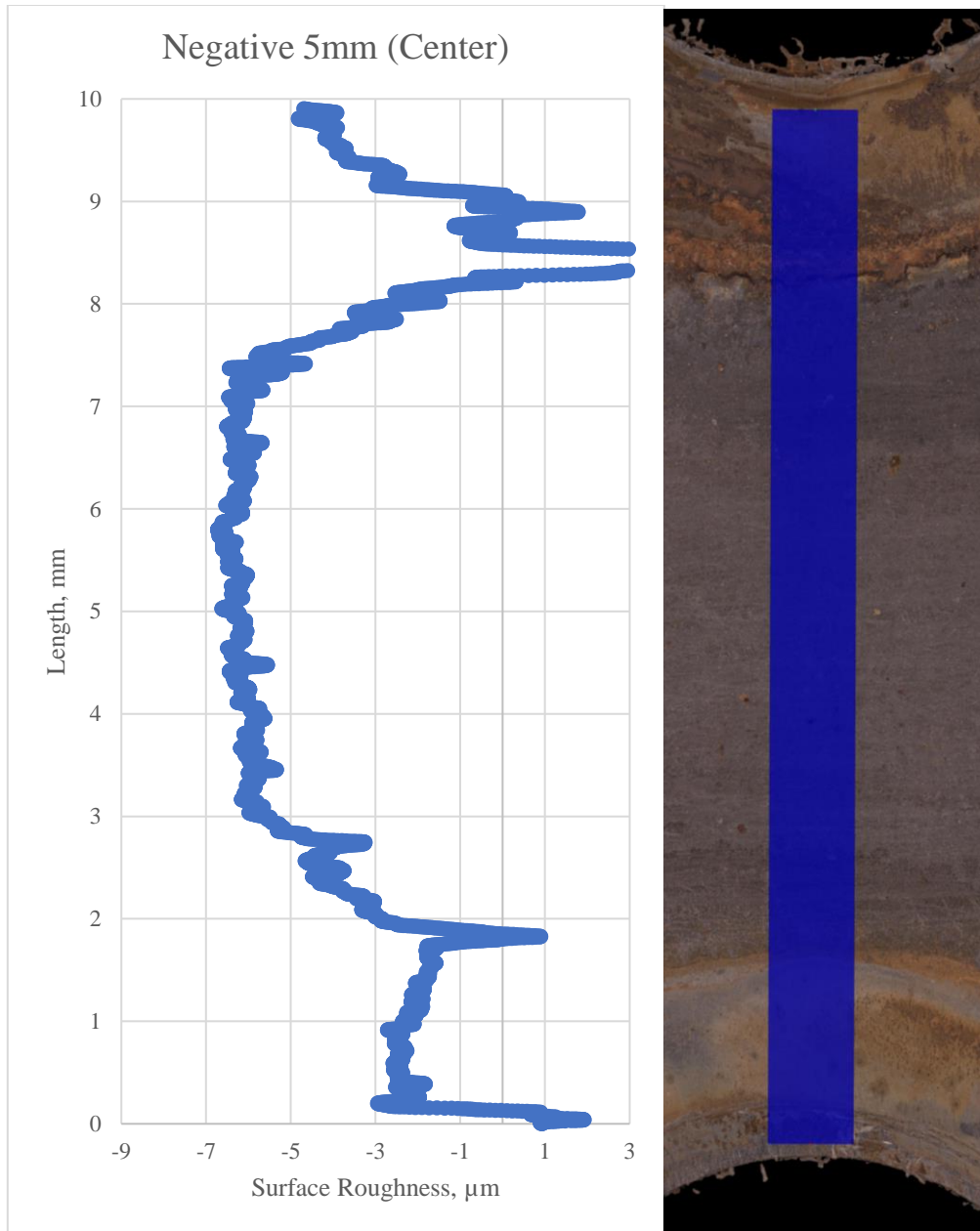


Figure 8: The above figures illustrate corrosion damage of the carbon steel of the in between the bolts of the Negative 5mm coupon using surface roughness measurements from the 3D microscope.

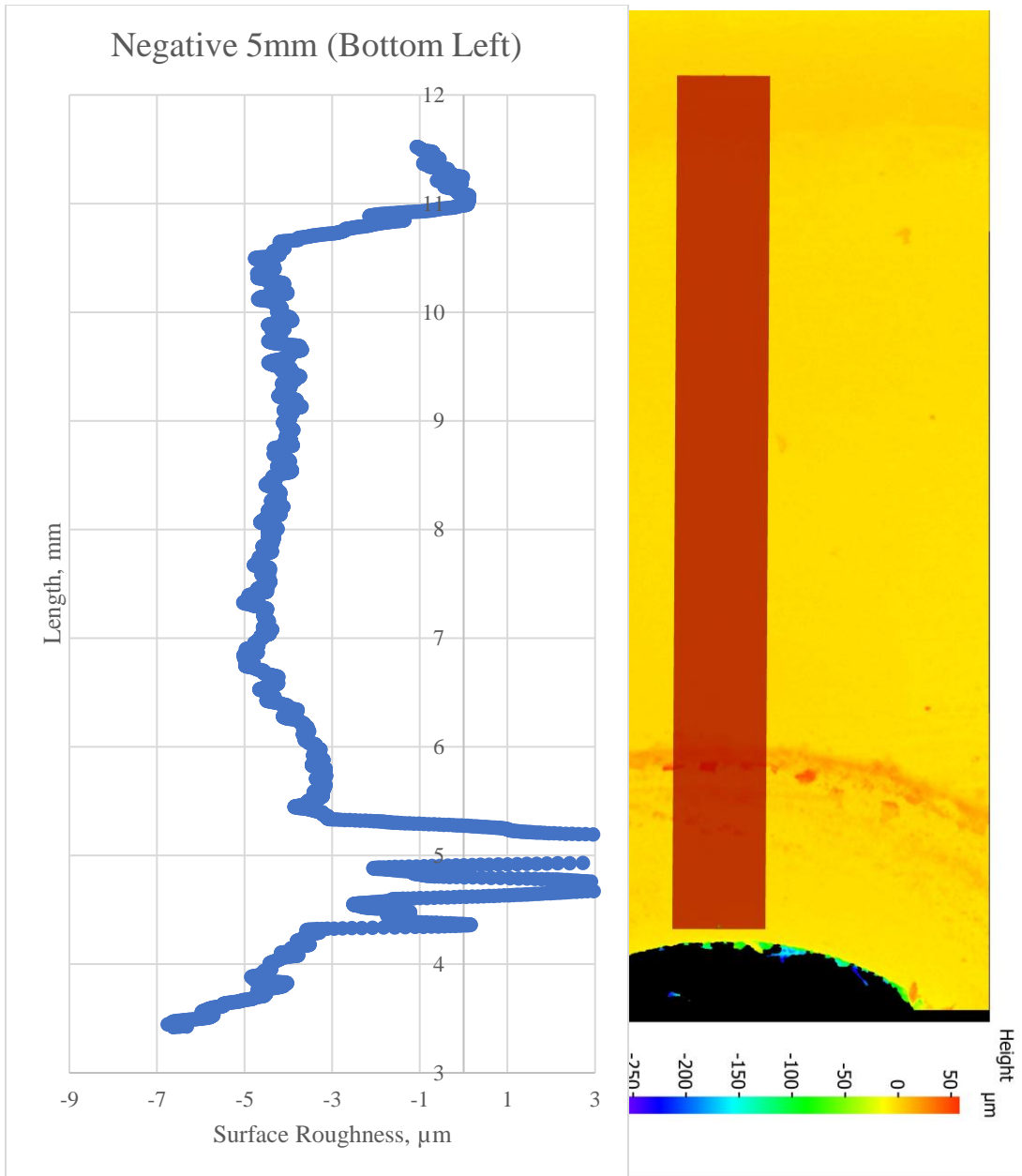


Figure 9: The above figures illustrate corrosion damage of the carbon steel of the bottom left portion of the Negative 5mm coupon using surface roughness measurements from the 3D microscope.

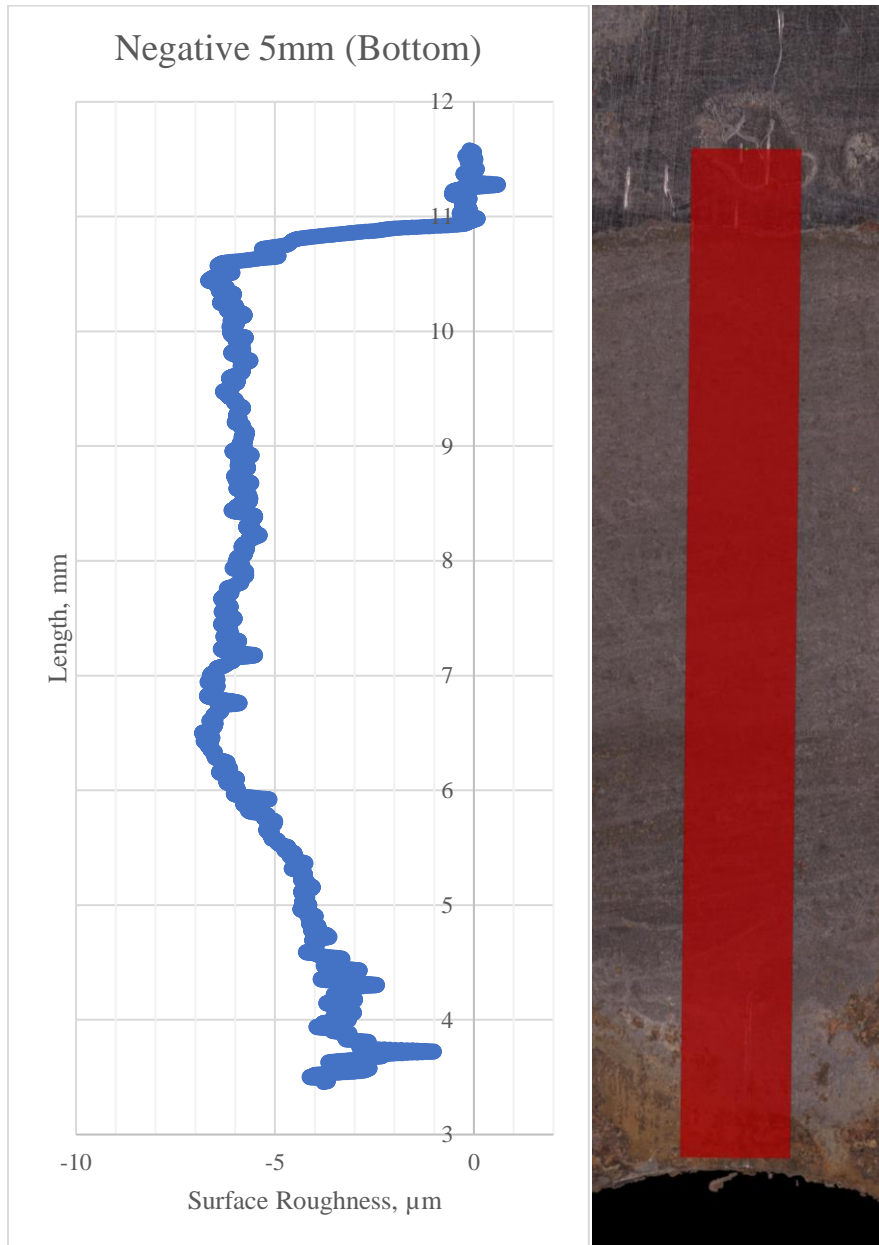


Figure 10: The above figures illustrate corrosion damage of the carbon steel of the bottom portion of the Negative 5mm coupon using surface roughness measurements from the 3D microscope.

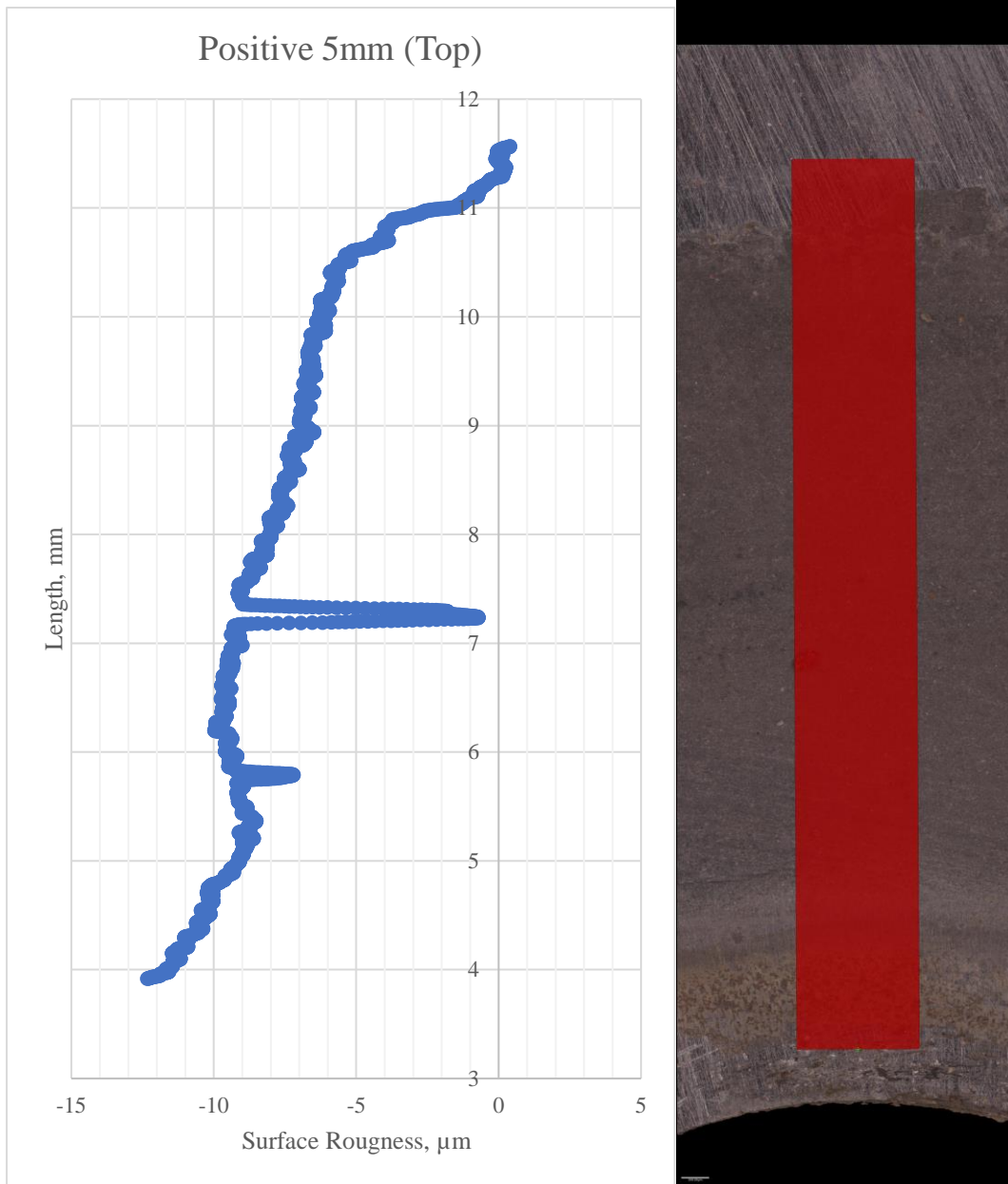


Figure 11: The above figures illustrate corrosion damage of the carbon steel of the top portion of the Positive 5mm coupon using surface roughness measurements from the 3D microscope.

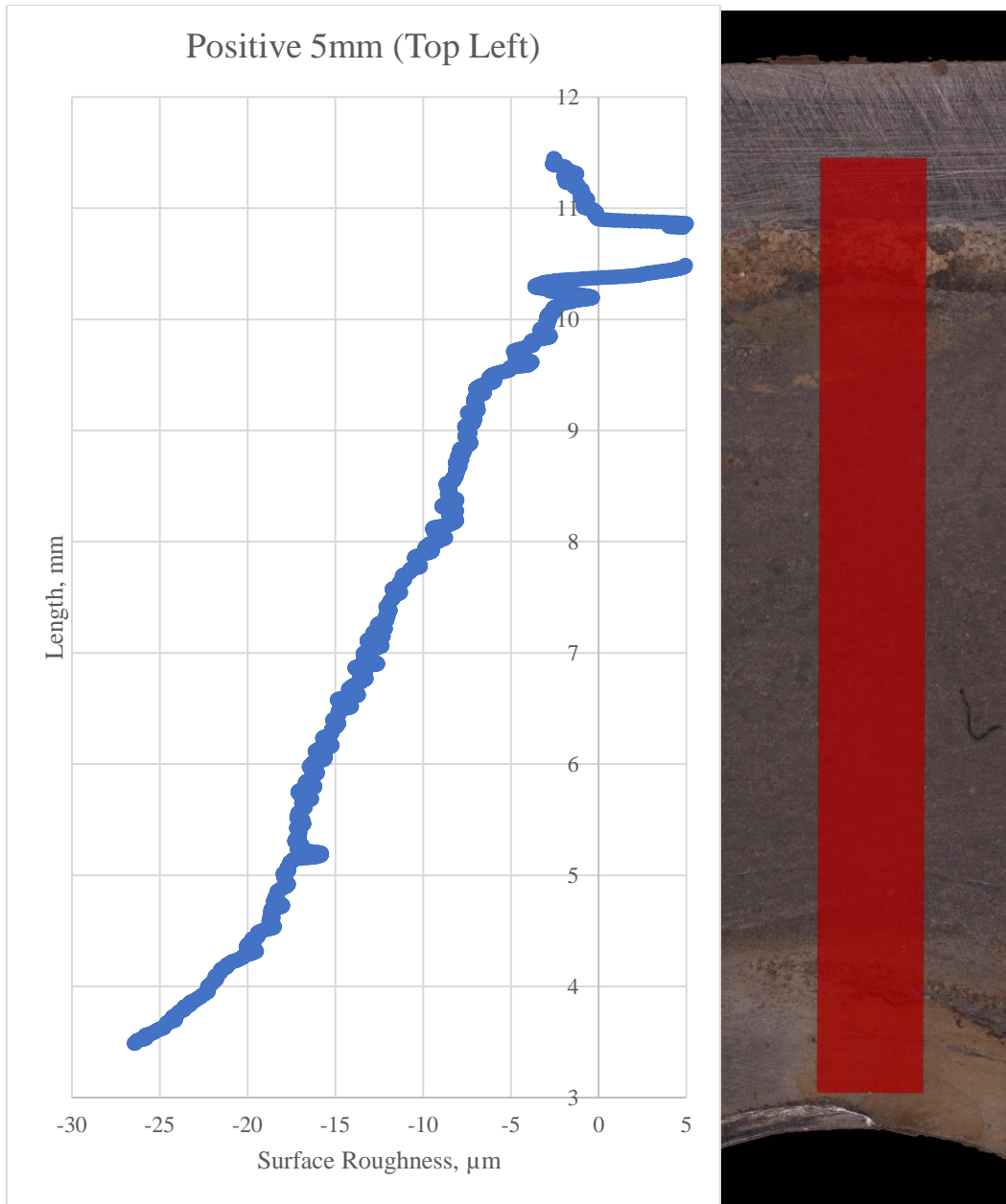


Figure 12: The above figures illustrate corrosion damage of the carbon steel of the top left portion of the Positive 5mm coupon using surface roughness measurements from the 3D microscope.

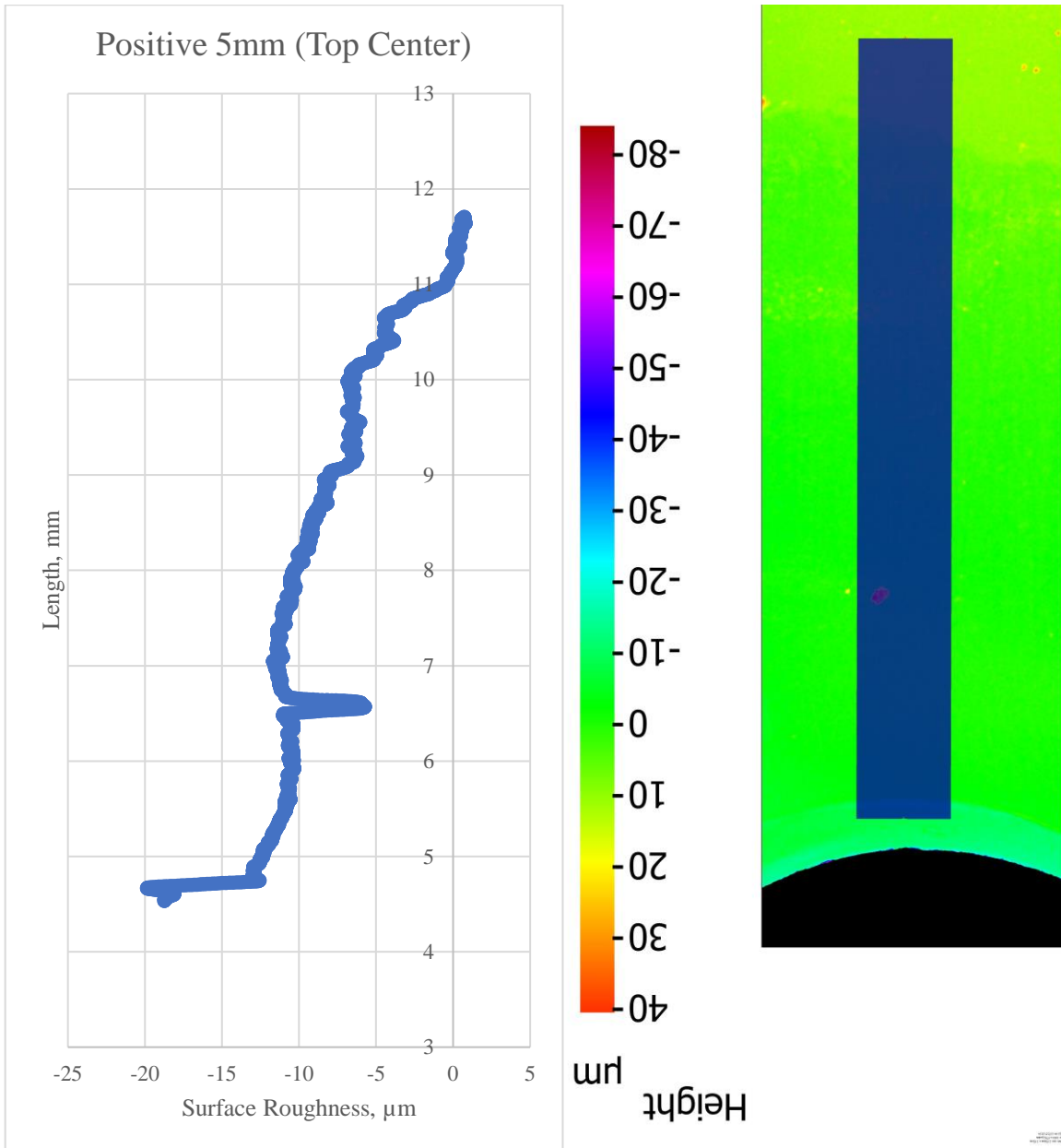


Figure 13: The above figures illustrate corrosion damage of the carbon steel in between the top bolt of the Positive 5mm coupon using surface roughness measurements from the 3D microscope.

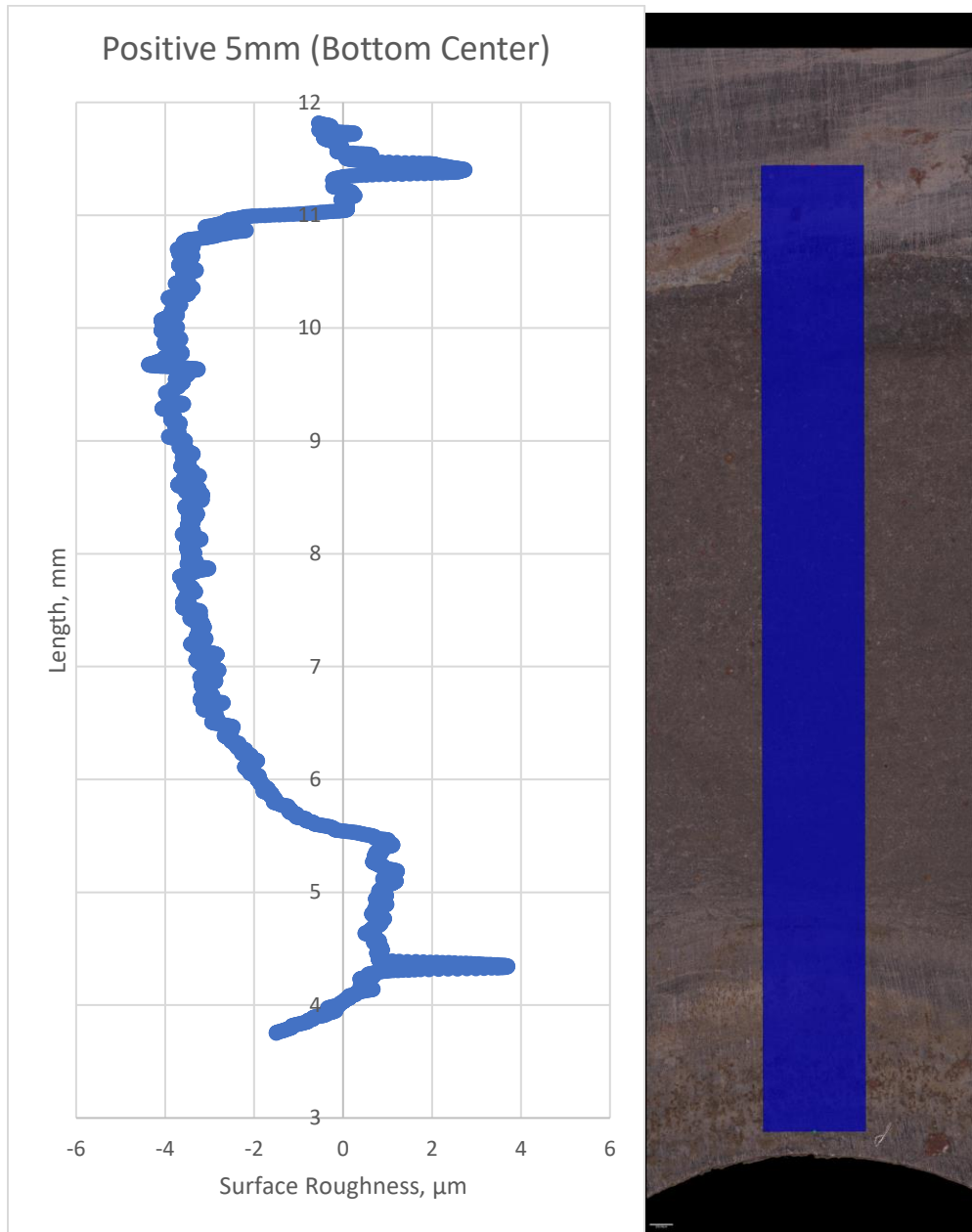


Figure 14: The above figures illustrate corrosion damage of the carbon steel in between the bottom bolt of the Positive 5mm coupon using surface roughness measurements from the 3D microscope.

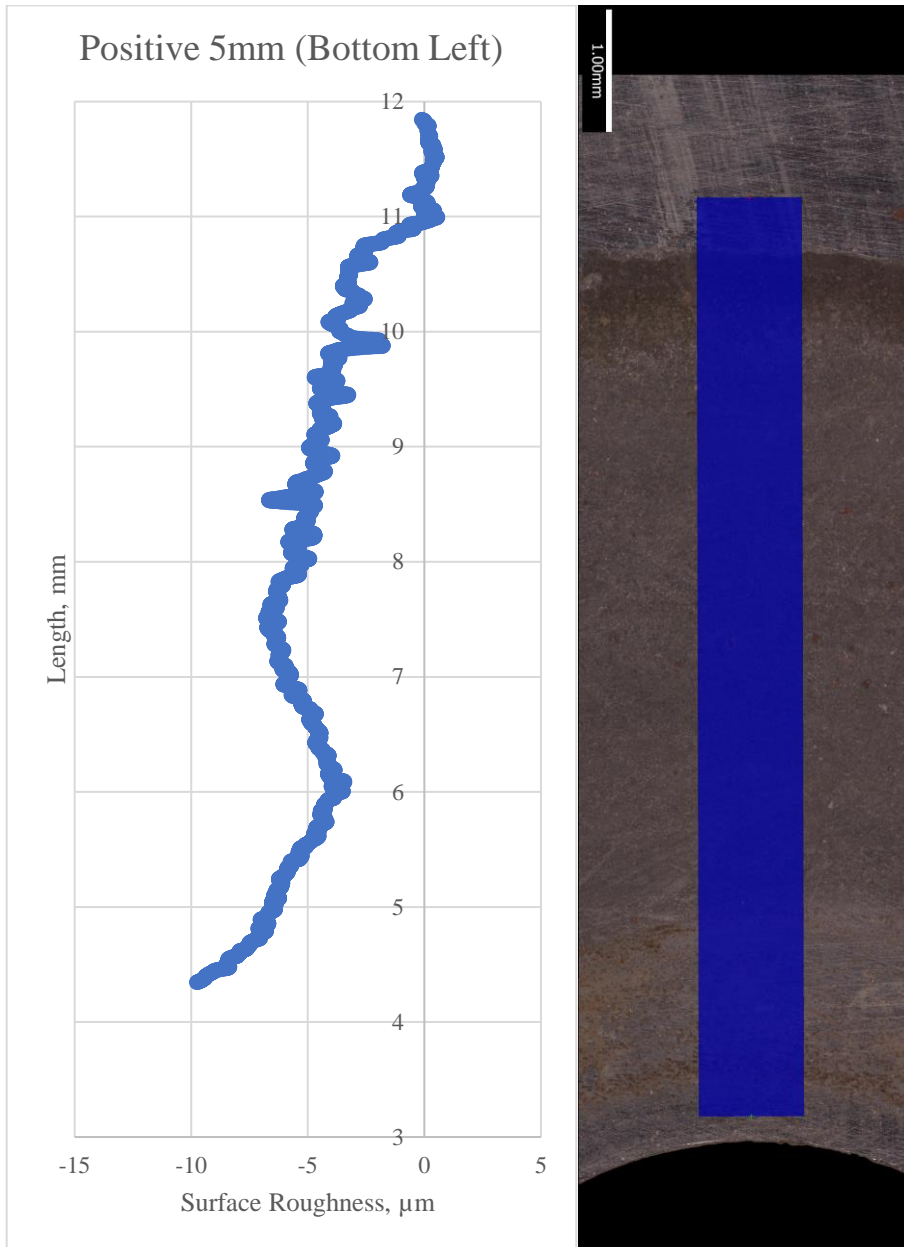


Figure 15: The above figures illustrate corrosion damage of the carbon steel of the bottom left side of the bolt of the Positive 5mm coupon using surface roughness measurements from the 3D microscope.

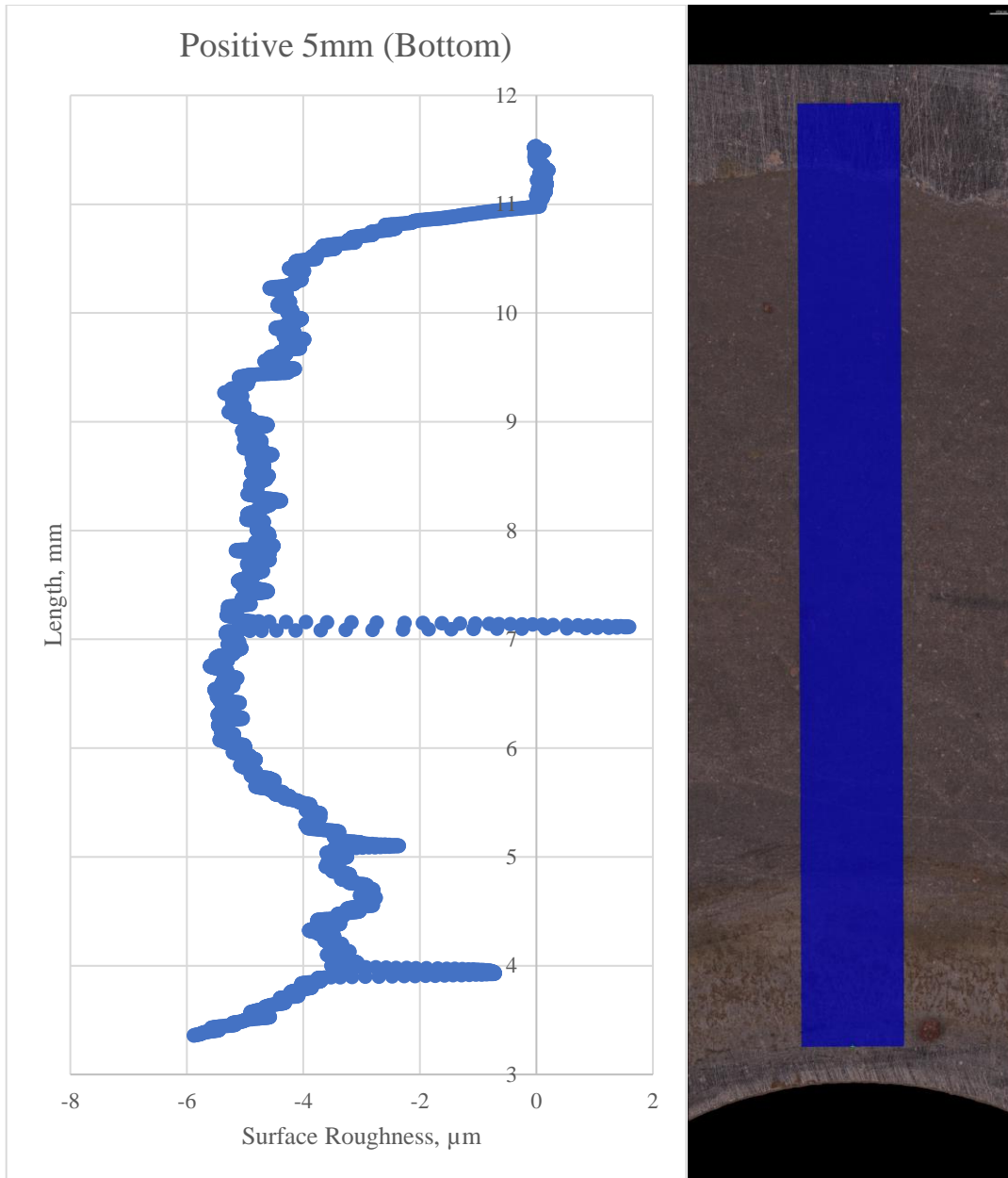


Figure 16: The above figures illustrate corrosion damage of the carbon steel of the bottom side of the bolt of the Positive 5mm coupon using surface roughness measurements from the 3D microscope.

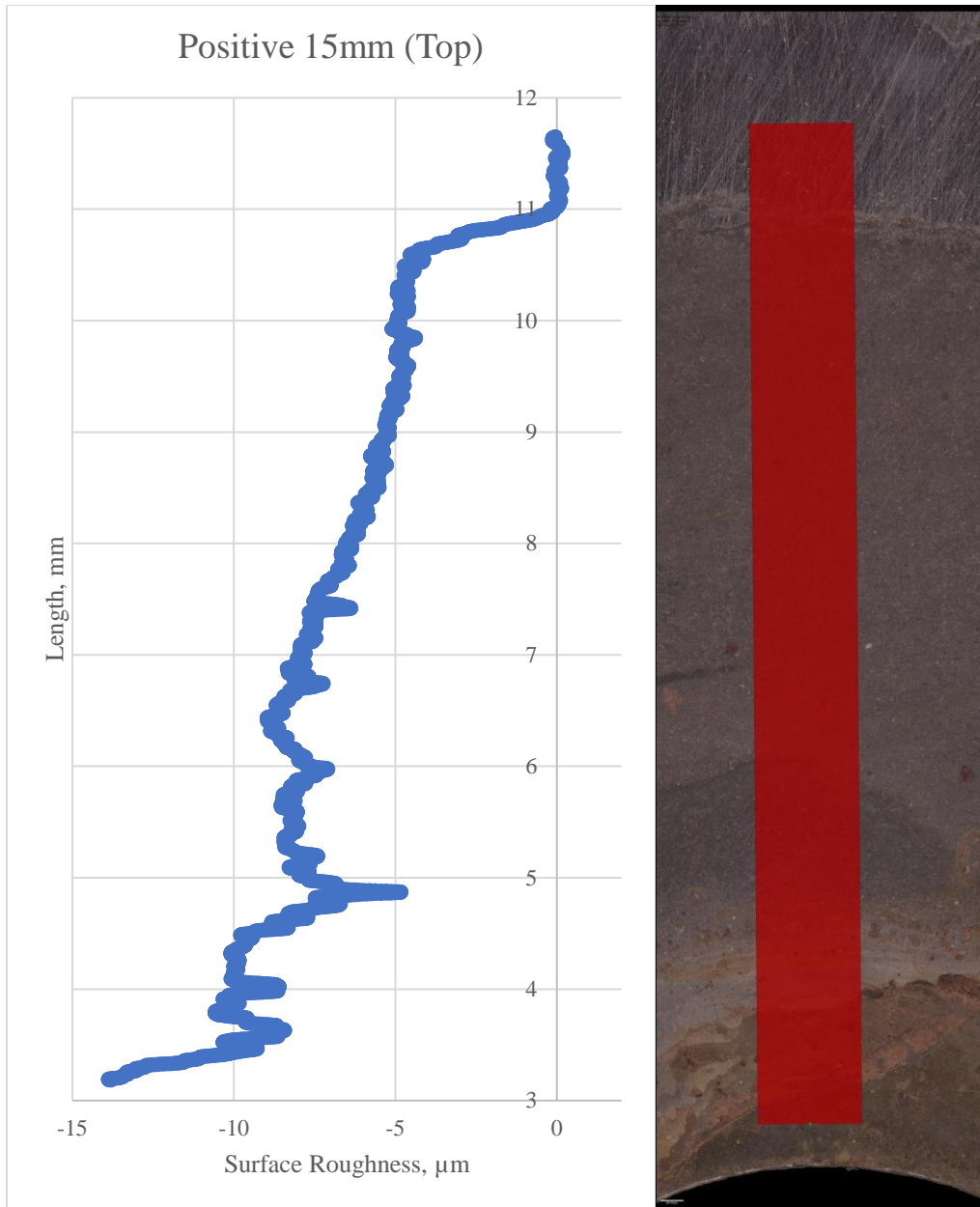


Figure 17: The above figures illustrate corrosion damage of the carbon steel of the top side of the bolt of the Positive 15mm coupon using surface roughness measurements from the 3D microscope.

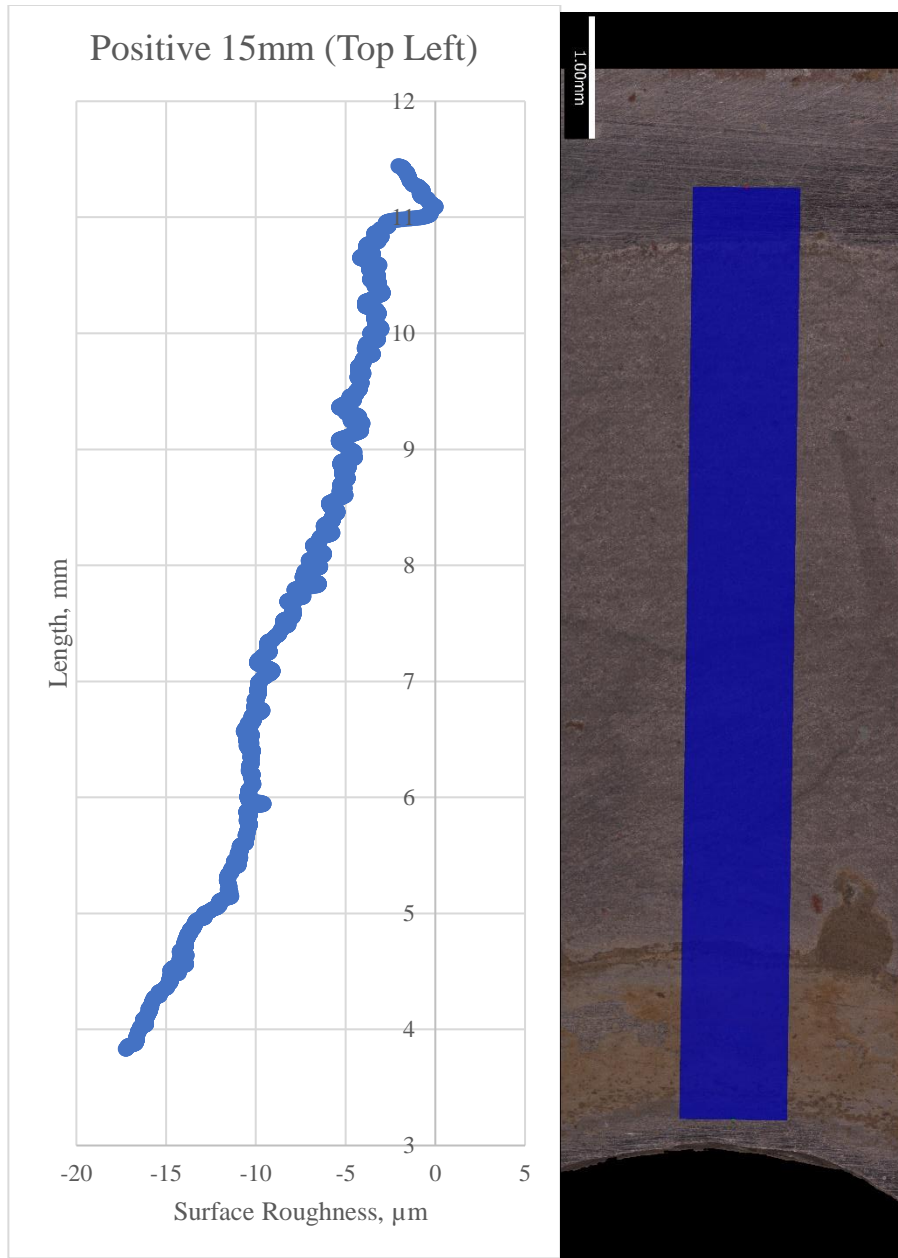


Figure 18: The above figures illustrate corrosion damage of the carbon steel of the top left side of the bolt of the Positive 15mm coupon using surface roughness measurements from the 3D microscope.

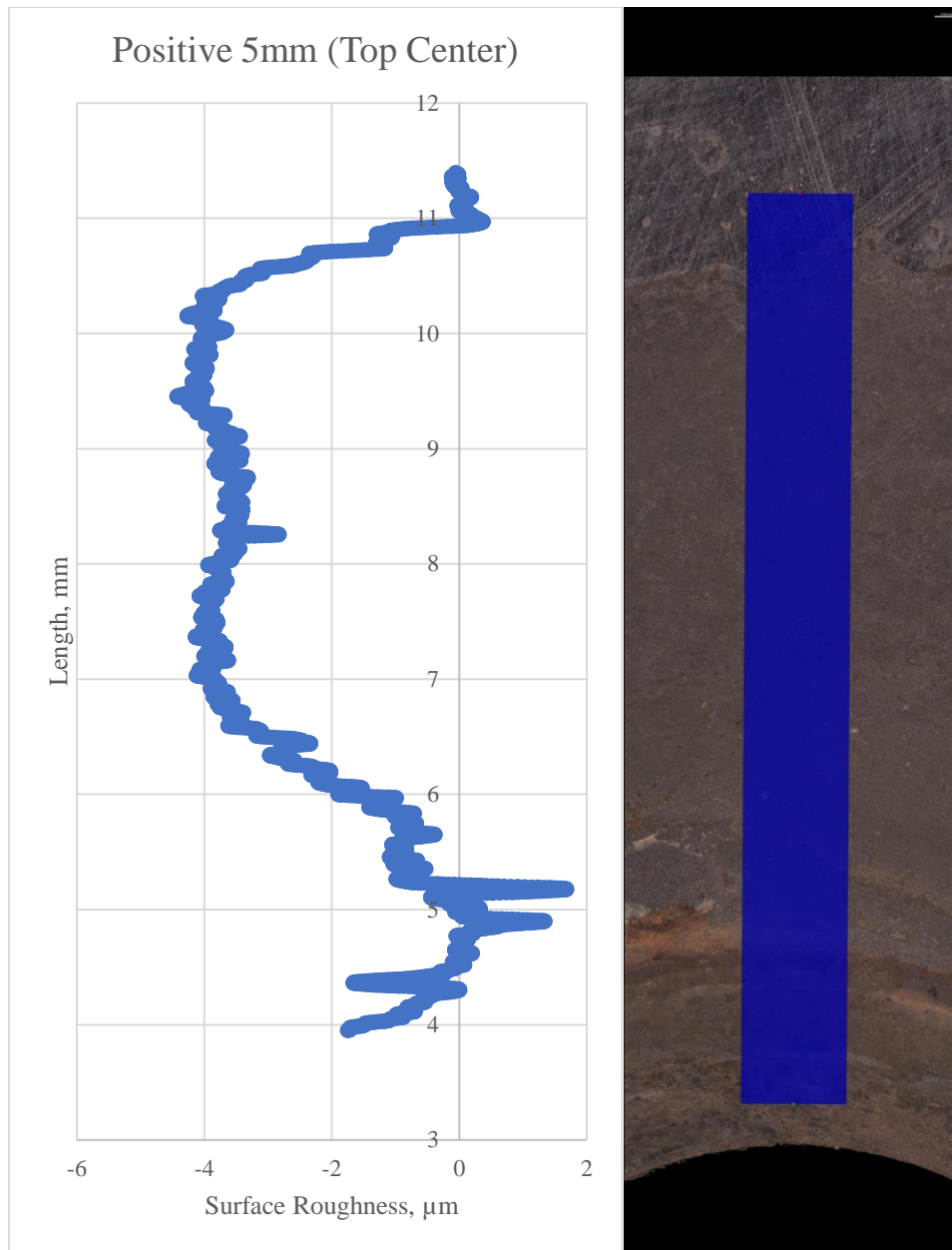


Figure 19: The above figures illustrate corrosion damage of the carbon steel in between the top bolt of the Positive 15mm coupon using surface roughness measurements from the 3D microscope.

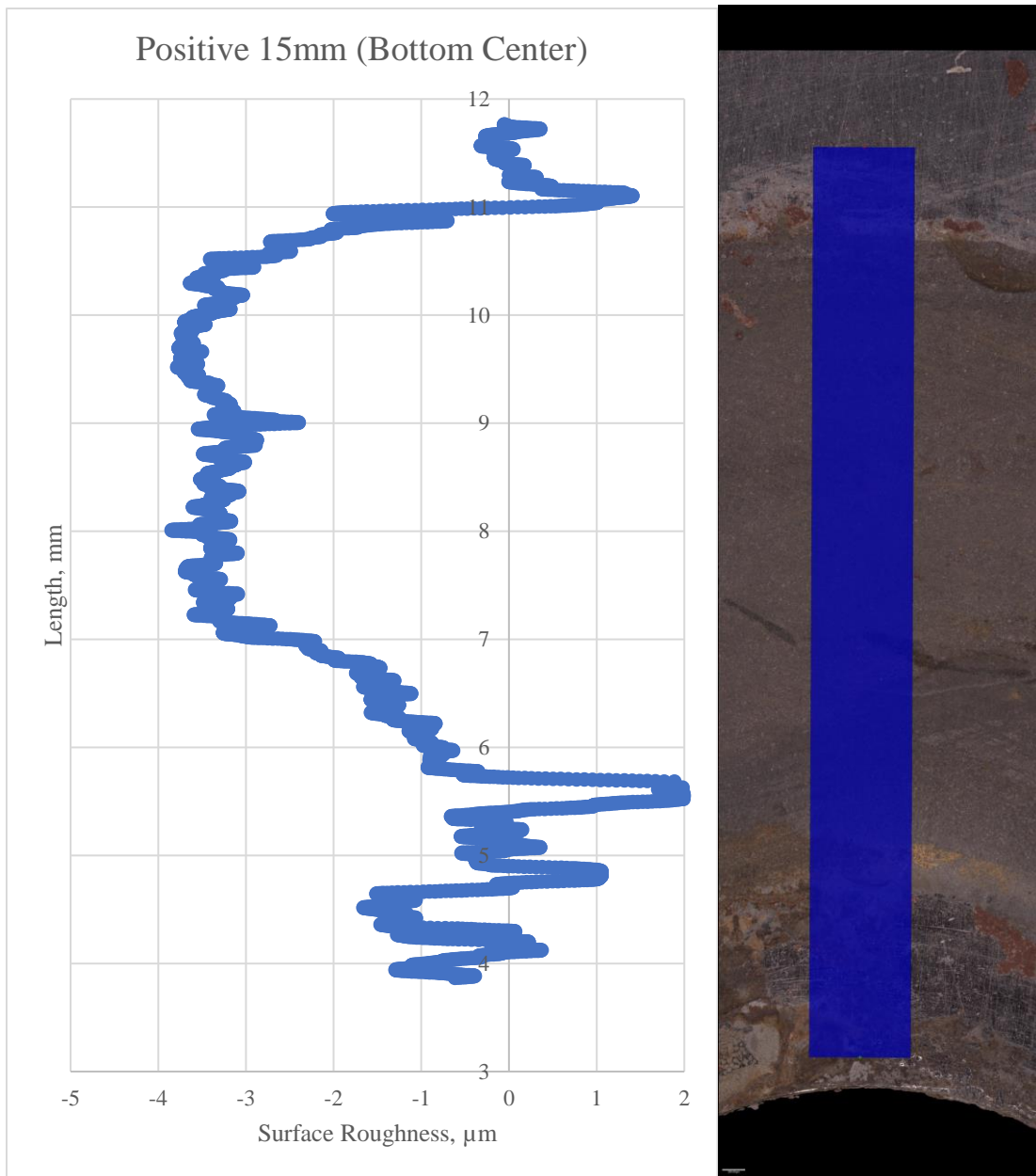


Figure 20: The above figures illustrate corrosion damage of the carbon steel in between the bottom bolt of the Positive 15mm coupon using surface roughness measurements from the 3D microscope.

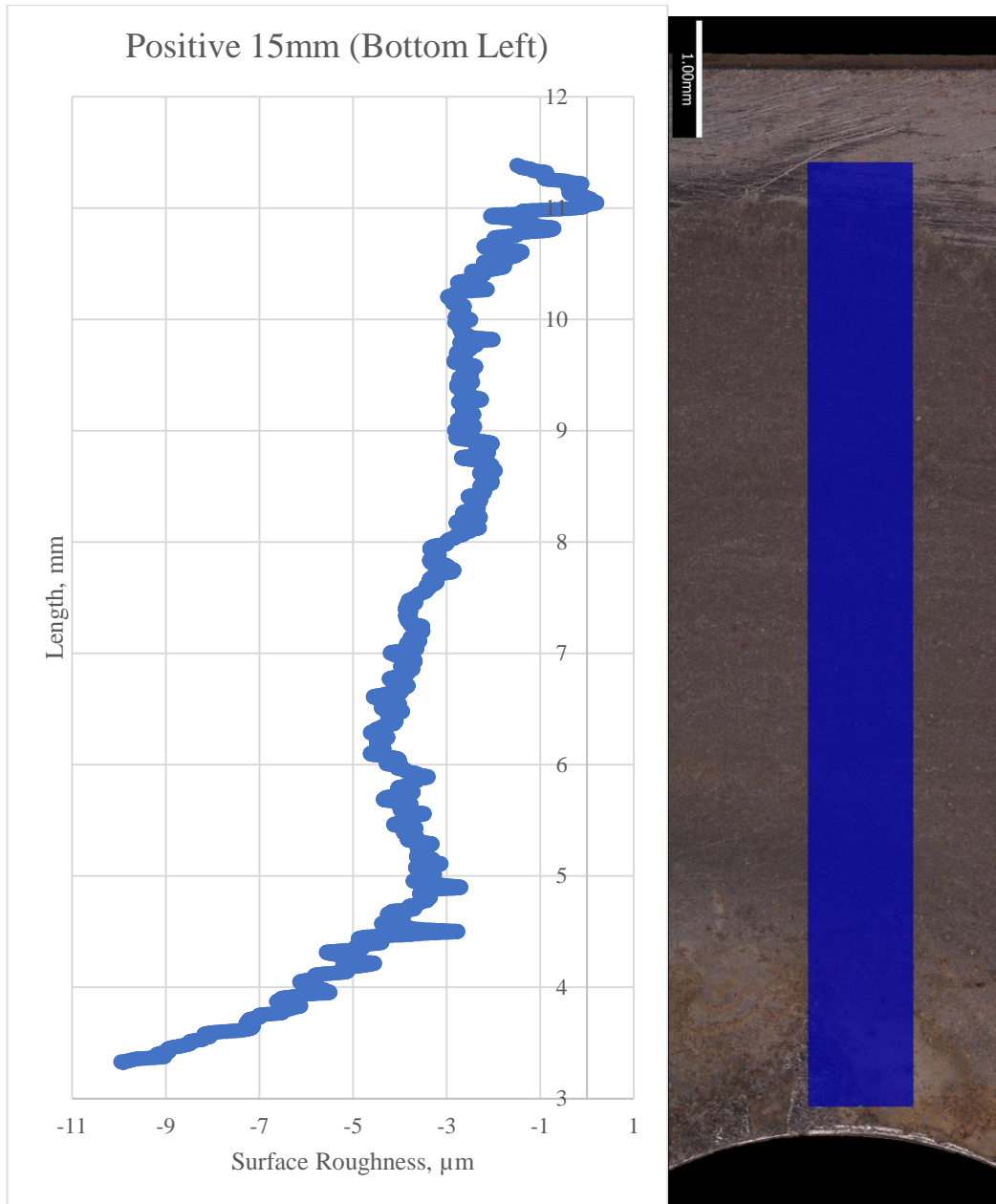


Figure 21: The above figures illustrate corrosion damage of the carbon steel of the bottom left side of the bolt of the Positive 15mm coupon using surface roughness measurements from the 3D microscope.

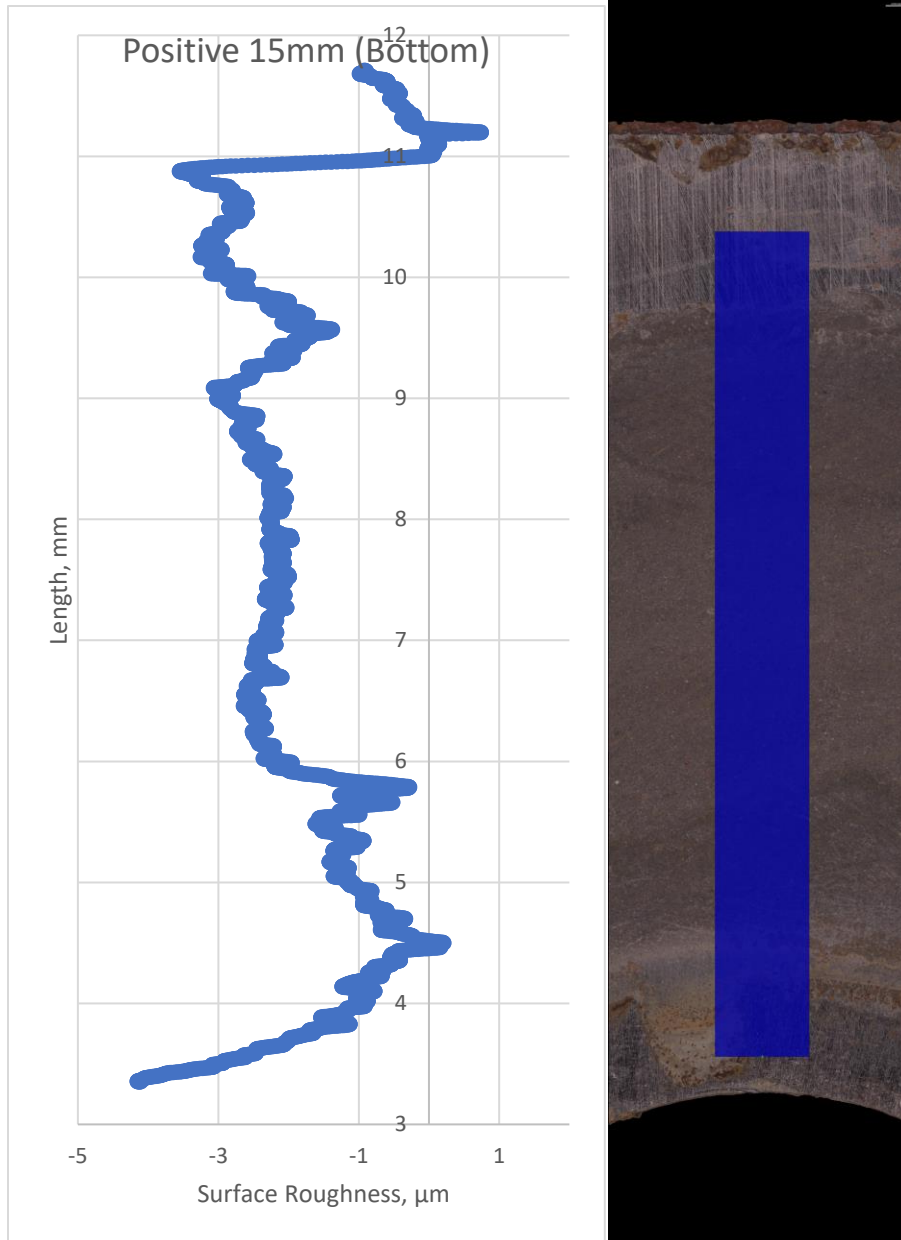


Figure 22: The above figures illustrate corrosion damage of the carbon steel of the bottom side of the bolt of the Positive 15mm coupon using surface roughness measurements from the 3D microscope.

Discussion

From the experiments a few trends were spotted from the results. The first trend is the mass loss calculated using the volume of a cylinder equation. The 3D microscope was able to measure the surface roughness of the coupons. The profile was normalized using a planar tool in the software of the 3D microscope. There was some difficulty in using the planar tool to normalize the profile of the surface for the data. From there the depth profile was normalized to set the uncorroded area equal to zero, then the linear length was adjusted, so that the edge of the corroded area was equal to the radius of the exposed area. Once the data was normalized, the volume of the corroded area was calculated by taking a summation of the volume of the cylinder using the surface roughness. It was assumed that the surface roughness profile for one scan direction was equal to the corrosion damage of one quarter of the corroded area. The area that the bolt contacted the steel plate was not used for calculating mass loss. The damage from the bolt was assumed to be caused by mechanical damage from tightening with the wrench and some crevice corrosion. Because of this only the corroded area beyond where the bolt interface was used in calculating mass loss. The mass loss calculated from the surface roughness calculated 13.2 mg for the single bolt specimen, 20.0 mg for the negative 5mm specimen, 23.9 mg for the positive 5mm, and 19.0 mg for the positive 15mm specimen. Seeing more mass loss from the two bolt coupons was anticipated and nearly double of the single bolt.

From the Tafel slope data, it is anticipated that the single bolt coupon should have a mass loss of 3.6 mg after an 8-day exposure. There should also be a mass loss of 6.18 mg for the 2-bolt specimen where area overlaps and 7.36 mg for the specimen with no overlap. These numbers were calculated using the point of intersection from the carbon steel and Monel Tafel plot as the anticipated corrosion rate and the known area of exposure for the coupons. The anticipated corrosion rate of the galvanic cell is $1.11 \times 10^{-5} \text{ A cm}^{-2}$. The data can be seen in **Figure 2** and **Table 3**. The calculated mass loss based on the Tafel plot was not equivalent to the mass loss calculated from the surface roughness. From the single bolt specimen, the sample had nearly $6 \mu\text{m}$ depth profile, which would equate to around 1.69 mm^3 of volume loss and 13.2 mg of mass loss. The measured mass loss from the 3D microscope is more than three times higher than the calculated mass loss from the corrosion rate of the Tafel slopes. The geometric spacing of the bolts did not seem to play a significant factor in accelerating corrosion rate at certain areas. There appears to be unique trends from the surface roughness measurements, but each profile appears to be unique and with little consistency. These errors from the 3D microscope could be attributed to the polishing or measurement procedure performed by the experiment operator.

Conclusion

From the results it appears that the corrosion rate determined from Tafel slopes is not completely equivalent to the mass loss measured with the 3D microscope. The 3D microscope shows trends that the corrosion rate is more than three times larger than that of the Tafel slopes. The 3D microscope can make precise measurements less than a micrometer, but ensuring the measurements are accurate relies on the principle that surface plane must be uniform, and the plane across the surface is flat after polishing. Any slight taper or angle will skew the results as the measurements being taken are less than a micrometer. The steel also appeared to corrode uniformly with some influence from the geometry of the bolt distance.

Works Cited

- [1] Hack, H. P., and J. R. Scully. "Galvanic corrosion prediction using long-and short-term polarization curves." *Corrosion* 42.2 (1986): 79-90.
- [2] Scully, J. R. *Bimetal and Multimetal Galvanic Corrosion Prediction Using Long-and Short-Term Polarization Curves*. DAVID W TAYLOR NAVAL SHIP RESEARCH AND DEVELOPMENT CENTER ANNAPOLIS MD SHIP MATERIALS ENGINEERING DEPT, 1984.
- [3] Hodgkiss, T., and C. W. Lim. "Aspects of galvanic corrosion behaviour of a range of materials in seawater." *Corrosion science* 35.1-4 (1993): 269-283.
- [4] Schleich, Wilhelm. "Application of copper-nickel alloy UNS C70600 for seawater service." *CORROSION 2005*. OnePetro, 2005.
- [5] McCafferty, Edward. *Introduction to corrosion science*. Springer Science & Business Media, 2010.
- [6] Jia, Ru, et al. "Microbiologically influenced corrosion of C1018 carbon steel by nitrate reducing *Pseudomonas aeruginosa* biofilm under organic carbon starvation." *Corrosion Science* 127 (2017): 1-9.
- [7] Dey, G. K., and P. Mukhopadhyay. "Precipitation in the Ni-Cu-base alloy monel K-500." *Materials Science and Engineering* 84 (1986): 177-189.
- [8] ASTM D1141-98, 2021, Standard Practice for Preparation of Substitute Ocean Water, American Society for Testing and Materials, ASTM International, West Conshohocken, PA.